TOWARDS SENSING AND PERCEPTION FOR AUTONOMOUS BERTHING – FORCE-TORQUE SENSOR AND AN ALGORITHM FOR THE GRIPPING POINT POSE ESTIMATION

Dymitr Osiński[(1)], Paweł Paśko[(1)], Michał Pawlak[(1)], Arkadiusz Łukasiak[(1)], Andrzej Jakubiec[(1)], Daniel Niewiarowski[(1)], Maciej Woźniak[(1)], Konrad Wszelaki[(1)], Łukasz Dudek[(1)]

[(1)] PIAP Space Sp. z o.o., al. Jerozolimskie 202, 02-486 Warsaw, Poland, Email:, dymitr.osinski, michal.pawlak, (pawel.pasko, arkadiusz.lukasiak, andrzej.jakubiec, daniel.niewiarowski, maciej.wozniak, konrad.wszelaki, lukasz.dudek)@piap-space.com

ABSTRACT

As more and more space missions that address the satellite de-orbiting, servicing, refuelling and in-orbit transportation are being prepared demand for robotic systems capable of supporting those functions increases. Polish aerospace company PIAP Space is developing key space robotic technologies that enable to achieve challenging goal by providing comprehensive and modular building blocks. This paper focuses on the development being conducted in the field of sensing and perception dedicated to an autonomous berthing and docking operation. The recently developed space grade 6 DoF force and torque sensor is described together with its calibration procedure and test results. Furthermore, an algorithm for the gripping point pose estimation is depicted followed by its test results. In conclusion the verification results serve as an indication for future development.

1 INTRODUCTION

Autonomous docking or berthing is an essential technology enabling in-orbit satellite servicing. While uncrewed docking is a well-established and widely used technology, autonomous robotic berthing technology employing multiple articulations was demonstrated just twice in ETS-VII [2] and Orbital Express [3] missions. In order to make robotic satellite servicing widespread, reliable and accessible key technologies, as well as, building blocks are needed. PIAP Space addresses this needs by executing several R&D projects aimed at developing and market crucial robotic technologies such as: robotic arm, grippers [4, 5] and sensors. While every robotic system is composed of actuation and control elements, sensing and perception are critical to enabling the autonomy of the system.

2 FORCE AND TORQUE SENSOR

The force and torque sensor is one of the key elements of general-purpose robotic arm systems and may as well be used for mobile robotics. For the berthing use case, it provides information to the robot control system about the contact event and the magnitude of the contact forces and loads exerted on the manipulator's tip. In the case of the direct docking, the sensor can be used as feedback for impact attenuation of the robot system. The contact phase is crucial for the berthing and docking operation as after contact the two bodies may rebound and separate, causing the failure to capture, therefore sensing this phenomenon is essential for making autonomous decision.

The sensor developed at PIAP Space belongs to a class of multi-axis force and torque sensors [6, 7] composed of a mechanical body equipped with strain gauges [8, 9, 10] that are redundant in this device. A dedicated custom-designed redundant electronic controller is fitted inside the body of the sensor. The controller converts analogue signals from strain gauge bridges to digital readings, decouples the signals [11] based on the sensor's characteristics from calibration [12, 13] and transmitting the measurements on the CAN bus.

2.1 Principles of operation

A six-axis force and torque sensor is a device that converts force and torque input $\boldsymbol{F}$ to signal output $\boldsymbol{U}$. The sensor measures three components of forces and three components of torques in $\mathbb{R}3$. The number of output signals depends on the design of the sensor.

$$\boldsymbol{U} \approx f(\boldsymbol{F}) \tag{1}$$

Where:

$$\boldsymbol{F} = [F_x \quad F_y \quad F_z \quad M_x \quad M_y \quad M_z]^T \tag{2}$$

$$\boldsymbol{U} = [U_1 \quad U_2 \quad \dots \quad U_n]^T \tag{3}$$

Typically, the six axis force and torque sensors based on strain gauges employ 6 or 8 Wheatstone bridges, due to that $n = 6$ or $n = 8$. At PIAP Space, sensors with 6 channels are being developed. Each signal output $\boldsymbol{U}$ is affected by each component of force and torque $\boldsymbol{F}$, as no sensor is perfectly decoupled. This is shown by the coupling matrix $\boldsymbol{C}$.

$$\boldsymbol{U} \approx \boldsymbol{CF} \tag{4}$$

Where:

$$\boldsymbol{C} = \begin{bmatrix} C_{11} & \cdots & C_{16} \\ \vdots & \ddots & \vdots \\ C_{n1} & \cdots & C_{n6} \end{bmatrix} \quad (5)$$

The output signal is assumed to be proportional to applied load, as the sensor is designed to operate in range of elastic deformations. Moreover, output signal is affected by a bias $\boldsymbol{E}$ that was not fully compensated. This offset is assumed to be constant in whole measurement range and different for each output.

$$\boldsymbol{E} = [E_1 \quad E_2 \quad \ldots \quad E_n]^T \quad (6)$$

Considering the above, the idealised transformation conducted by a sensor can be expressed as:

$$\boldsymbol{U} = \boldsymbol{CF} + \boldsymbol{E} \quad (7)$$

A simple transformation can be done to estimate forces and torques acting upon sensor when the coupling matrix $\boldsymbol{C}$ is invertible.

$$\boldsymbol{F} = \boldsymbol{C}^{-1}(\boldsymbol{U} - \boldsymbol{E}) \quad (8)$$

In this case it is done as the sensor uses the same number of strain gauge bridges as there are outputs, i.e., $n = 6$. This operation can be employed in order to use the force and torque sensor as a measurement instrument. In the calibration process, the values of the coupling matrix $\boldsymbol{C}$ and the bias matrix $\boldsymbol{E}$ are obtained.

2.2 The sensor in scope of ORBITA and TITAN Projects

The six-axis force and torque sensor for space applications is developed at PIAP Space in the ORBITA project. The aim of the project is to develop robotic building blocks including a family of modular grippers for orbital and planetary applications, sensors, and vision algorithms. The sensor will also be employed in the TITAN project that pertains to development of a robotic arm for satellite servicing. An Engineering Model of a multi-articulated robotic arm will be made for future missions involving deorbiting and servicing of in-orbit satellites. The force and torque sensor is to be placed between the 7th joint and the end effector on the TITAN manipulator (Fig. 1). The sensor will enable sensing loads acting upon the manipulator and allow detecting contact between the end effector and gripped object. Moreover, the sensor will enable active back-driving by compliant force and torque control of motion.

The most important requirements define measurement range of 50 N and 50 Nm, overload capacity of 300%, redundancy, vacuum compatibility (10-6 Torr) and operating range of -40/+100°C (survival range is -100/+125°C). The initial accuracy requirement is ≤3% of full-scale reading of the whole measurement chain. Remaining requirements limit the size (diameter smaller or equal to 200 mm), maximum mass (1,5 kg), power consumption (no more than 5 W) and other parameters.

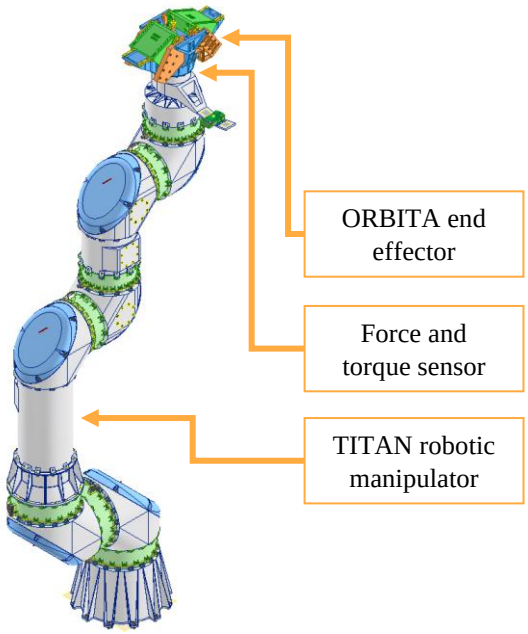

Figure 1. TITAN manipulator with LARIS Gripper and force and torque sensor.

The redundancy requirement is fulfilled by employing a single mechanical structure of the sensor and equipping it with two sets of independent strain gauge bridges. This allows to save mass and volume, capitalising on the higher reliability of mechanical structure above electronic components. Both sets of strain gauge bridges are connected to individual, independent parts of controller with separate communication and power connections.

A DM-1 off-the-shelf Force and Torque Sensor produced in Europe by commercial supplier was acquired. A design resembling Stewart platform was chosen thanks to its low non-linearity, high accuracy and advantageous ratio of stiffness to mass. The parameters of the sensor were close to required, especially the overall dimensions, mass of the sensor as well as accuracy and measurement range for torques. There were some exceptions such as large measurement range for forces.

After a series of tests with measurement range limited to 50 N for forces and 50 Nm for torques the performance of the sensor was deemed satisfactory. A custom

mechanical structure with strain gauge bridges of DM-2 sensor was ordered from the same manufacturer (Fig. 2). The requirements for this sensor were set by PIAP Space. The sensor is to have measurement range of 50 N and 50 Nm, be fitted with redundant measurement channels, is to be vacuum compatible and suitable for extended temperature range. The sensor is larger than off-the-shelf due to the need for fitting the controller electronics inside, as well as, providing detachable covers and sensor's housing.

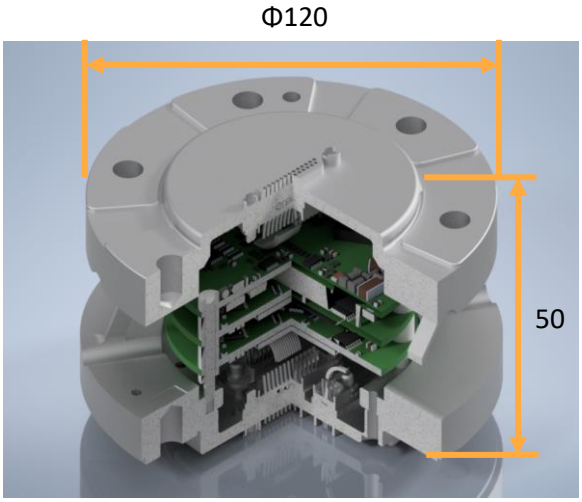

Figure 2. Force and torque sensor DM-2.

2.3 Electronic and software layers of the sensor

PIAP Space developed a custom electronic controller for six axis force and torque sensors. The BB model of the controller used mostly simple analogue components and was used to operate off-the-shelf sensor during validation and verification phase. The main PCB contains microcontroller that receives measurement signals after they have been amplified and offset. Analogue to digital converters were used to transduce the signals that were then transmitted on a CAN bus. Original controller from the manufacturer of the sensor was used to verify the accuracy of the measurements made with the BB model. Separate circuit was employed as a switch between both controllers. A coupling and bias matrices were employed to translate the signals from voltage drops to forces and torques. The controller operated properly and positively verified the approach.

Next iteration of the controller is being developed. It consists of three PCB stacked one above other in order to fit inside the FTS and is prepared to use space rated components (Fig. 3). First DM model that uses commercial components was manufactured and is being tested. The controller was initially used with off the shelf sensor to verify its operation. The results were positive, and it will be installed in custom sensor manufactured for PIAP Space. Besides driving the strain gauge bridges, the controller is able to read temperature sensors and power heaters used in thermal stabilisation system of the sensor.

Figure 3. PIAP Space force and torque sensor controller.

A proprietary software for driving the controller, permitting data acquisition and visualisation, was developed (Fig. 4). The software allows display of the measurement results in human-readable format, logging the measurements in typical .csv file with a timestamp, setting relative reference, adjusting communication frequency, setting averaging window and more. The calibration data consisting of coupling and offset matrices are imported to enable calculation of forces and torques acting upon the sensor based on signals from the strain gauge bridges. The software currently employs CAN bus for communication and operates on Windows and Linux (Ubuntu 18.04) operating systems. Embedded version that employs CANopen is being developed.

Figure 4. PIAP Space Controller user interface.

2.4 Calibration of the sensor

PIAP Space has also developed setups for verification of the readings and calibrating force and torque sensors by applying known forces and torques. A small prototype workbench was developed to verify this method (Fig. 5).

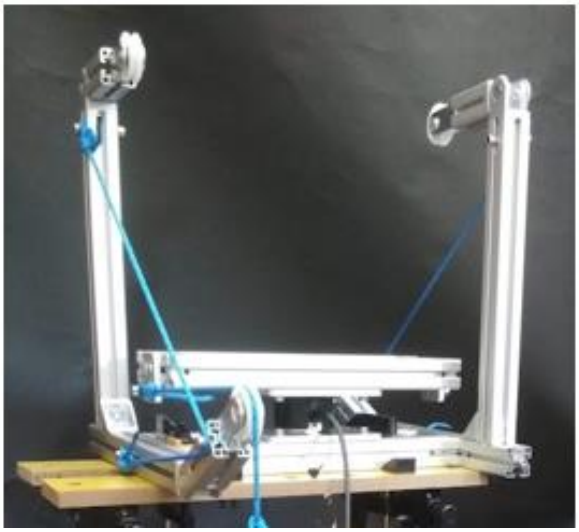

Figure 5. Prototype calibration workbench.

The results were satisfactory and larger calibration station was developed (Fig .6).

The station allows applying loads simultaneously in multiple axes and is compatible with climate chamber at the premises of PIAP Space. The station is equipped with precisely machined weights, two calibrated dynamometers (Axis FC-00 with H3-C3/200kg sensors calibrated to 1 kN tension) and employs pulley system to apply forces and torques to the sensor in order to verify its measurements and to allows conducting calibration. The sets of weights allow for application of loads from 15 N or 7,5 Nm up to 800 N or 400 Nm. No load scenario is also possible, and the range can be expanded or fine-tuning by adding appropriate weights. The calibration results contained in coupling and bias matrices are then used in software to translate the voltage signals to readings of forces and torques. Parts of the station can be swapped to allow for calibration of different sensors.

The station was used to verify the readings of the off the shelf sensor under different temperatures and later will be used to measure the thermal effects on the DM-2 sensor in order to allow for the thermal compensation.

During calibration each axis of the sensor is calibrated in positive and negative directions with clean force and torque loads of known magnitude and direction. The relation between force or torque load change and electric signals from strain gauges change is then approximated with a linear function (Fig. 6). The approximations are then used to form the coupling matrix $\boldsymbol{C}$. During the calibration a known absolute load is placed on the sensor in order to calculate the bias matrix $\boldsymbol{E}$.

Numerous calibrations were conducted to test and verify stability. The COTS sensor exhibited high linearity in the tested range (typically $R^2 \geq 0{,}99$). A part of the variation of results is caused by testing different approaches to calibration, such as using higher or lower number of test points or applying loads only the in positive or negative directions.

A climatic chamber at the premises of PIAP was used to conduct thermal tests of the Force and Torque Sensor. The sensor was tested in the available range of the climatic chamber, from -50 to 50°C, and survived without issues. Moreover, calibrations at temperatures of -20, 0, 20 and 40°C were conducted. The results indicated that the coupling matrix $\boldsymbol{C}$ is not affected by the temperature significantly due to analogue thermal compensation employed, while the values of bias matrix $\boldsymbol{E}$ change proportionally to change in temperature.

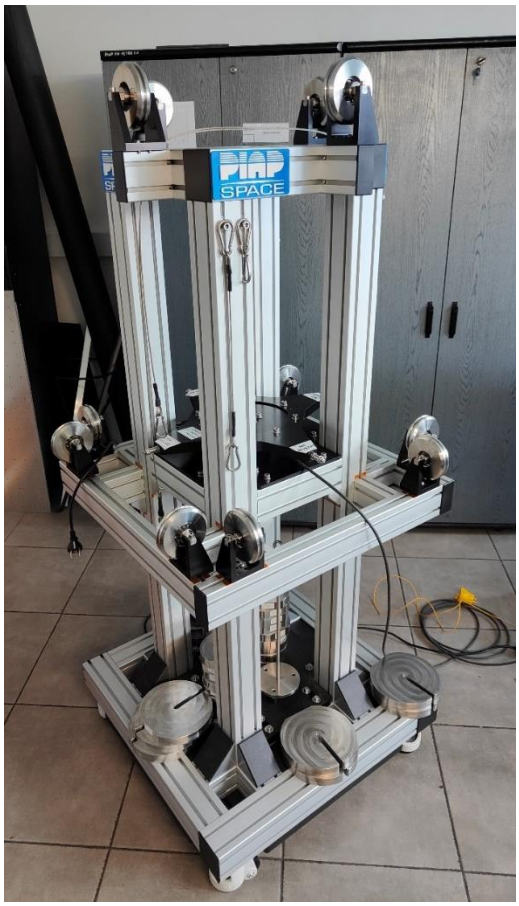

Figure 6. PIAP Space force and torque sensor calibration station

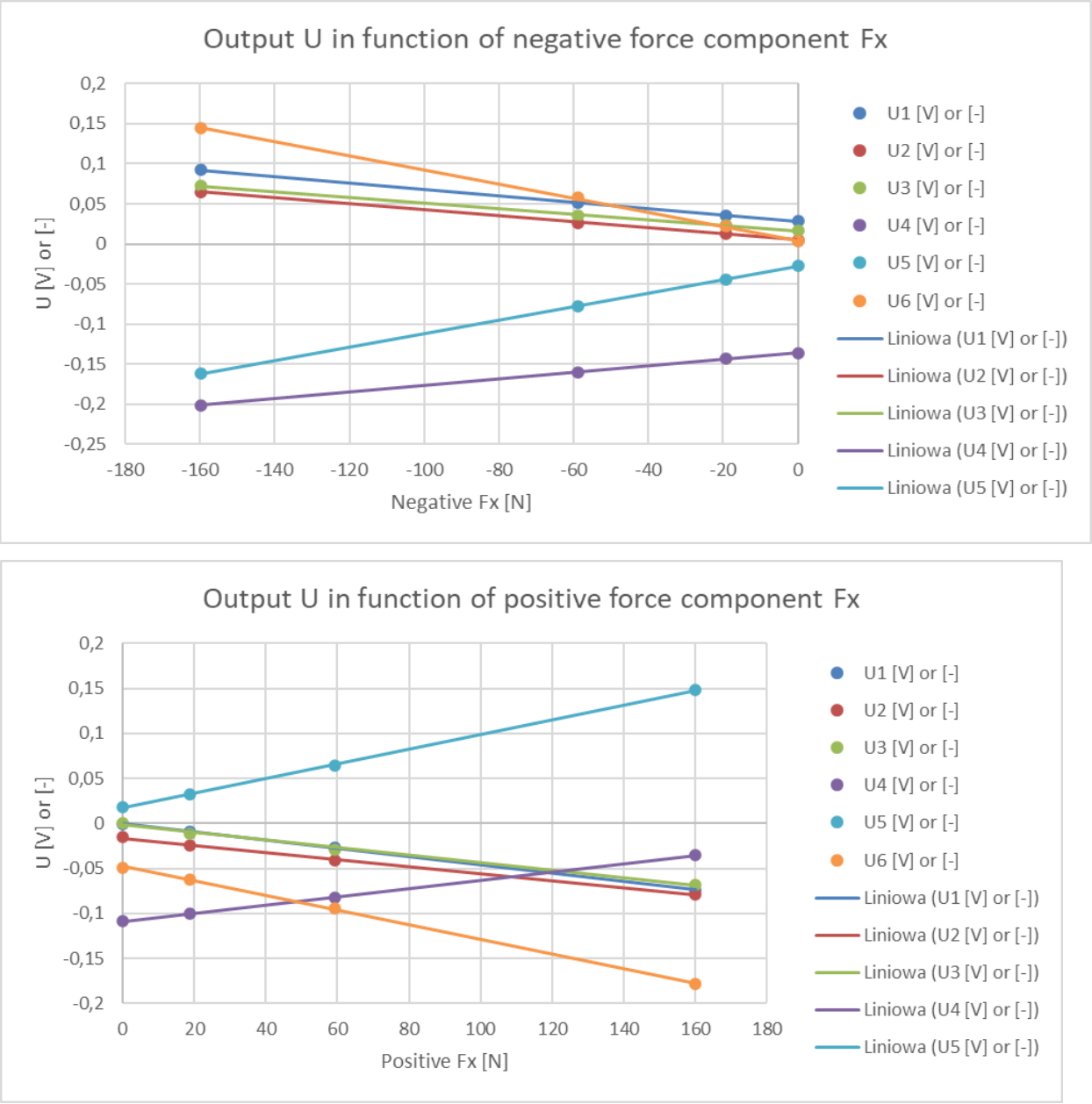

Figure 7. Example of calibration results for pure X axis force loads.

2.5 Discussion of the calibration approach and initial results

It appears that the developed calibration method has numerous advantages and a couple of disadvantages. The disadvantages may be improved in future.

The method employed accounts for the phenomena of coupling and allows to acquire the coupling matrix during calibration process. The coupling matrix can be then used to decouple output signals and obtain information about force and torque components acting upon the sensor. During calibration pure forces or torques are applied and output signals are read. No complex loading is necessary. Complex loads may be used to verify calibration results.

The method for obtaining the coupling matrix $\boldsymbol{C}$ employs changes of outputs corresponding to changes in loads during calibration which allows to neglect constant loads.

Using least square methods fitting allows to obtain lowest average error in the whole measurement range. The mathematical operations are simple and quick to compute. Complex mathematical operations are not needed, not even for solving a linear equation system.

The proposed calibration may be used for sensor with any number of outputs (provided it is equal to or larger than the number of inputs). During single calibration involving applying known forces and torques to the sensor, the parameters of redundant sensor channels can be simultaneously read, allowing for calibration of both without increasing time nor workload. The calibration is also not exclusive to the kind of strain gauge for forces and torques. It can be used for any kind of force and torque sensor with linear output, e.g., an optical sensor that employs fibre Bragg gratings [14]. No knowledge of any parameters of sensor besides number of outputs is needed.

Thermal characteristics are measured and then used for determining load applied to the sensor. Compensation is provided both for components independent on load and dependant on load.

The calibration process assumes that changes in output of the sensor are proportional to changes to its input. It is a common assumption for strain gauge-based force and torque sensors. Should it generate too large errors, the calibration may be expanded to use polynomials of higher degree instead of linear functions.

Ill-conditioned coupling matrix may cause small deviations to produce big changes in results after inversion. It is possible to avoid matrix inversion by using neural networks for signal processing, though it seems to be expensive computationally and difficult to validate for space applications. The inversion of matrix must be done only once after the calibration is finished.

The calibration assumes static conditions and provides no information about dynamic response of the sensor. A dynamic test to determine bandwidth may be attempted.

The calibrations are conducted at different temperatures and between those temperatures the values of the coupling matrix $\boldsymbol{C}$ and bias matrix $\boldsymbol{E}$ are interpolated. This is considered as a feasible workaround in order to avoid the need for conducting a large number of full calibrations yet obtain necessary thermal parameters that are accurate enough.

The calibration is conducted by operators that hang appropriate weights on the calibration station. This means that the possible calibration environment is limited by the human operators, e.g., can't have extreme temperatures or vacuum. This may be solved by introducing a system of actuators, ideally compatible with large range of temperatures and vacuum.

3 VISION SYSTEM

Autonomous robotic perception system is addressed in the paper through the gripping point pose estimation algorithm. The algorithm is part of a vision system for a robotic arm that is designed for capturing unprepared satellites. The algorithm detects and determines the position on the Launch Adapter Ring (LAR) that is to be grappled by the dedicated mechanism. The readings are used in the motion control to properly position the gripper with regards to the LAR. Low accuracy, instabilities or poor performance of the vision system could result in suboptimal behaviour of the whole robotic arm and could threaten the success of the capturing tasks.

The main task of the vision system is to obtain linear position and angular orientation of LAR with regard to the camera matrix, which can be later transformed to the reference frame of the gripper. The advantage of the designed algorithm is that it functions without the whole LAR being in the camera's field of view, it does not need any optical or different markers and it functions with single Time of Flight (ToF) camera. It's LAR agnostic, however, it does require prior information about the LAR's diameter and height. Additionally, the algorithm can start execution at any position regarding LAR if it is visible and defines position of closest griping point even if it is outside FoV of the camera, however, other griping points can be estimated as well. Assumed accuracies increase as the distance to the target decreases, starting from 20 mm at 1,2 m distance and reaches 4 mm at 0,25 m distance.

3.1 Current algorithm design

The algorithm is developed from several function blocks (Fig. 8) and is mainly based on the fact that each point in cloud data from the camera has a known exact position in 3D space in the camera reference frame. The Point Cloud Library [16] functions have been used inside the algorithm. After initial cloud data filtration (removing data that are numerically useless) the plane of the tracked satellite is estimated and information on the LAR orientation is obtained. Results are used to set the cloud perpendicular to the sensor. With that step and taking into account LAR specification the algorithm performs data filtration along the z-axis to retrieve data describing visible LAR fragment. Data at a close distance to LAR could be distorted so another filtration is applied (clustering). With clean LAR data the algorithm estimates the position of the LAR centre point using the equation of the circle together with statistical analysis and information about the LAR diameter. With information about the LAR centre point the algorithm

finds the edge of the satellite that is closest to the visible LAR and estimates its angle and calculates the gripping point.

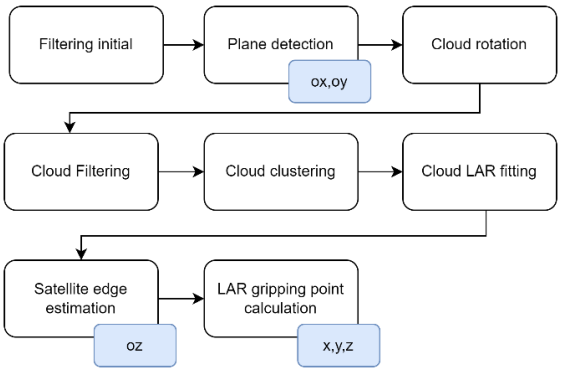

Figure 8. Overview of the vision system algorithm steps, with outputs produced at every step.

To reduce impact of noisy data, the moving average filter with removing disturbed data has been applied. The Fig. 9 below presents the LAR fit (bigger cylinder) and gripping point (big white point) imposed on the RAW data cloud and results of intermediate steps of the algorithm (after cloud rotation and after estimation of LAR centre point).

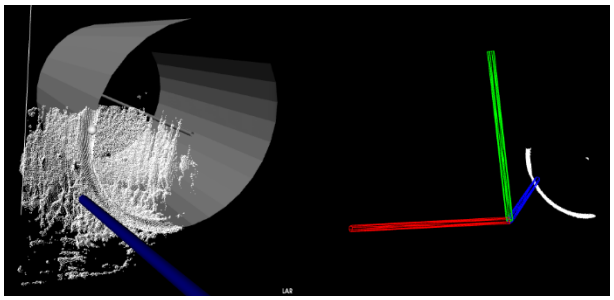

Figure 9. RAW point cloud data from camera with visualized estimated LAR

The vision system's hardware is composed of S100D CubeEye camera module with U300 bridge board from Meere company and a Jetson module Aetina AIE-CT41 with Nvidia Jetson TX2 NX. The S100D is a 3D Time-of-Flight (ToF) camera with Samsung S5K33DXX sensor. The specific type of ToF sensor uses so called continuous wave (CW) modulation, also known as CW phase-shift or Indirect Time of Flight. Selection of the camera type on this stage was dictated by the compactness of the assembly rather than readiness of space equivalent components, however attempts to qualify this kind of cameras has been done in the past [17]. On the other hand, the Nvidia Jetson selection was motivated by the availability of radiation-characterized module [18].

3.2 Test setup and tools

For validation of assumed functionality and accuracy the 3x3x3 m setup bench was built and covered with material [15] with strong IR absorption (Fig. 10). The purpose for this material is to absorb light from ToF emitter which after being reflected could be detected as a construction wall. The camera is mounted on a rail and a tripod head so it can be moved independently in all 6 degrees of freedom. The 3D printed version of Sentinel-3 LAR with reflective foil (Mylar and Mylar+Kapton) is placed on a wall in front of the camera. A manual coordinate measurement machine (CMM) is used to verify accuracy in all 6 degrees of freedom.

Figure 10. Test bench for VS validation

3.3 Test procedure

PIAP Space team has performed first verification of developed vision system to check its performance. The tests were planned to check accuracy of the gripping point position and orientation estimation by moving the camera towards LAR in the assumed range and to compare algorithm results with the CMM ones. For each single measurement position more than 400 single vision system measurements were taken with 30 Hz sampling. The results presented as difference between CMM and vision system readings are shown in the charts below. Moreover, PtV values from Vision System (VS) readings are presented. The camera resolution has been decreased to 320x240 as it did not improve any measurement accuracy or stability but reduced calculations frequency.

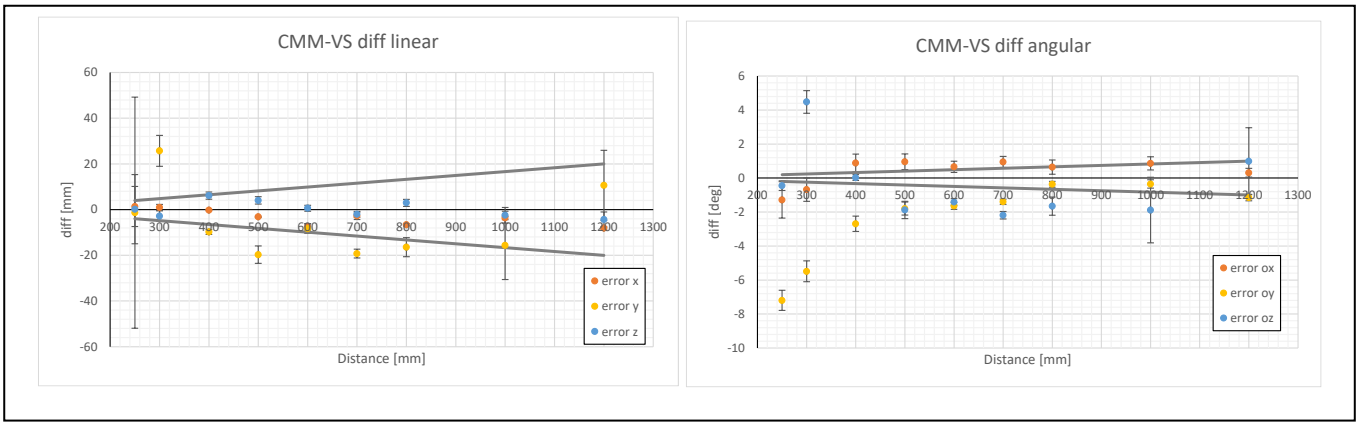

Figure 11. Difference between VS results and CMM readings of grasping point pose estimation on linear and angular axis, grey lines describes required accuracy.

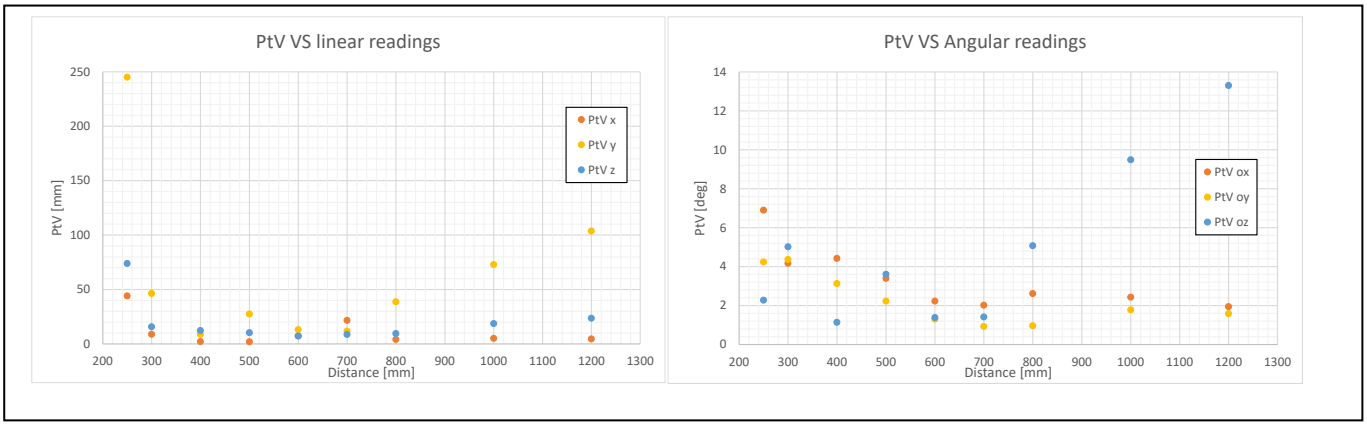

Figure 12. PtV values of VS readings in function of distance to LAR.

3.4 Test results and conclusions

The results presented above show that mostly for whole measurement range linear readings are below required values. The readings below 250 mm are not presented because of algorithm instabilities. Additionally, below distance of 400 mm for linear and 500 mm for angular readings the errors and PtV values are increasing. This can be corrected by implementation of different algorithm which will only calculate geometric centre of points from LAR. The other problem found on short distances is lack of satellite edge in FoV of the camera which is used to estimate oZ axis. This could be solved using second camera with wider FoV or setting the nominal camera further on a robotic arm. The PtV values potentially could be reduced by implementing more aggressive filters, however high instabilities on y-axis are caused by the measurement configuration – y axis is tangent to LAR in most measurements.

Further development is planned to improve the algorithm and perform more detailed tests with artificial light and robotic arm.

4 CONCLUSION

Two development and engineering models of the Force Torque Sensor were successfully developed, with the FTS EM being currently tested. The planned scope of the tests includes performance, vibration and TVAC testing to reach TRL6. In the future, it is intended to develop a method and equipment to calibrate the FTS in under extreme temperatures.

The Vision System is currently tested in order to tune the parameters and determine the characteristics of accuracy for more test cases including the tilted position of the camera, different lighting conditions and different MLIs. The system will be used during the functional testing campaign of the TITAN manipulator. As for the future further development is planned in order to define and implement a path to flight of the system.

5 ACKNOWLEDGMENTS

This publication is the result of the project “Development of the family of modular grippers for orbital and planetary applications – ORBITA”. The project is co-

financed by the European Regional Development Fund under the Smart Growth Operational Programme contract number POIR.01.01.01-00-0464/20-00.

6 REFERENCES

1. PIAP Space. Online at *www.piap.space* (as of 28 April 2022).
2. Kawano, I., Mokuno, M., Kasai, T., Suzuki, T. (2001). Result of autonomous rendezvous docking Experiments of Engineering, Test Satellite-VII, *Journal of Spacecraft and Rockets*.
3. Friend R. B. (2008). Orbital Express program summary and mission overview, *Proc. SPIE 6958, Sensors and Systems for Space Applications II*..
4. Janusiak, P., Jakubiec, A., Kleszczynski, D., Kraciuk, I., Osiński, D., Pawlak, M., Pukacz, A., Trojnacki, M. (2022). Modular Robotic System for Future Servicing and Deorbiting Missions, *Proc. Clean Space Industry Days (CSID) – ESA-ESTEC, Noordwijk, The Netherlands*.
5. Osiński, D., Kraciuk, I. (2022). A Multipurpose Gripper Concept and Preliminary Architecture for On-orbit Servicing Missions in *16th Symposium on advanced space technologies in robotics and automation (ASTRA), Noordwijk,*
6. Templeman, J. O., Sheil, B. B., Sun, T. (2020). Multi-axis force sensors: a state-of-the-art review. *Sensors and Actuators A: Physical*, vol. 304.
7. Song, A., Liyue, F.U., (2019). Multi-dimensional force sensor for haptic interaction: a review. *Virtual Reality & Intelligent Hardware*, vol. 1, no. 2, pp. 121-135.
8. Hoffman, K. (1989). An Introduction to Measurements using Strain Gages. Hottinger Baldwin Messtechnik GmbH, Darmstadt.
9. Strain Gage Based Transducers. Their Design and Construction (1988). Ed. the Technical Staff of Measurements Group, Inc., Measurements Group, Inc., Raleigh, North Carolina, 27611, USA.
10. Keil S. (2017). Technology and Practical Use of Strain Gages With Particular Consideration of Stress Analysis Using Strain Gages. Wilhelm Ernst & Sohn, Berlin, Germany.
11. Han, B., Lia, Y. (2016). Research of current studying status and developing trend of decoupling algorithm for six-axis force/torque sensor. International Conference on Advanced Electronic Science and Technology (AEST 2016), pp. 638-642.
12. Schleichert, J., Rahneberg, I., Fröhlich, T. (2013). Calibration of a novel six-degree-of-freedom force torque measurement system. Measurement of Mass, Force and Torque (APMF 2013*), International Journal of Modern Physics: Conference Series*, vol. 24.
13. Chen, D., Song, A., Li, A. (2015). Design and Calibration of a Six-axis Force/torque Sensor with Large Measurement Range Used for the Space Manipulator. *Procedia Engineering*, vol. 99, pp. 1164-1170.
14. Huang, J., Wong, C.Y., Pham, D.T., Wang, Y., Ji, C., Su, S., Xu, W., LIU, Q., Zhou, Z., (2018). Design of a Novel Six-Axis Force/Torque Sensor based on Optical Fibre Sensing for Robotic Applications. International Conference on Informatics in Control, Automation and Robotics.
15. IR flock sheet material specification. Online at *https://www.the-black-market.com/marketplace/ir-flock-sheet* (as of 20 March 2023).
16. Open source project for point cloud computing. Online at *https://github.com/PointCloudLibrary/pcl* (as of 12 April 2022).
17. Uno, K., Burtz, L-J., Hulcelle, M., Yoshida, K. (2017). Qualification of a Time-of-Flight Camera as a Hazard Detection and Avoidance Sensor for a Moon Exploration Microrover, Trans. JSASS Aerospace Tech. Japan, Vol. 16, No. 7, pp. 619-627
18. https://aitechsystems.com/product/s-a1760-space-gpgpu/